Synthesis, Spectroscopic and Biological Activities Of Complexes Of 2-[(3-Chlorobenzylidene) Hydrazinylidene]-1,2-Diphenylethanimine

Sharad Sankhe[1*] and Krupali Shah[1]

[1]Department of Chemistry, Patkar-Varde College, Goregaon West, Mumbai-62, India.

Abstract

This study provides the synthesis of the mononuclear complexes of 2-[(3-Chlorobenzylidene)hydrazinylidene]-1,2-diphenylethanimine ligand (HBMH*m*CB). We have used elemental, spectral, X-ray, and magnetic moment investigations to characterize all of the compounds. Oximino ions have monodentate coordinated with the metal ions, according to the infrared spectra. This coordination takes place at the $O_2N_2Cl_2$ donor sites of deprotonated oximino single bond OH, as well as at the imine N atoms of hydrazone and aromatic chloro group. Octahedral geometry is shown by spectroscopic and magnetic investigations of the Ni(II), Fe(II), Co(II), Mn(II), and Cu(II) complexes. While complexes with Zn(II), Hg(II), and Cd(II) exhibit tetrahedral geometry, Pd(II) possesses square planar geometry. The antimicrobial and cytotoxic properties of freshly synthesized compounds were studied. The complexes are effective against a wide variety of bacteria and yeasts, including *C. albicans*, S. cerevisiae, *B. subtilis, P. aeruginosa*, and *E. coli*. The HBMH*m*CB ligand and its complexes exhibited a wide range of cytotoxic properties.

Keywords: α-Benzilmonoxime, Hydrazides, Chlorobenzaldehyde, Cytotoxic properties

INTRODUCTION:

α-Benzilmonoxime is typically produced through the reaction between benzil, a diketone, and hydroxylamine [1]. The resulting product features a monoxime functional group (-N(OH)-) covalently bonded to a benzil framework. Used as a reagent in diverse organic synthesis reactions, α-benzilmonoxime's monoxime functional group actively engages with various functional groups, thereby facilitating the creation of novel compounds [2-3]. Beyond its applications in organic synthesis, α-benzilmonoxime has found utility in research endeavors aimed at exploring reaction mechanisms, kinetics, and other facets of organic chemistry [4-6]. Furthermore, investigations into certain compounds related to α-benzilmonoxime have been conducted to assess their potential biological activity [7-9]. However, obtaining specific details on this aspect may necessitate consulting the most recent scientific literature.

The hydrazide functional group, characterized by a carbonyl group connecting two nitrogen atoms (-$CONHNH_2$), imparts distinct reactivity to hydrazides [10], rendering them adaptable in a variety of chemical reactions. This unique structure broadens the applications of hydrazides across organic synthesis, medicinal chemistry, materials science, and biological research [11-13]. Their multifaceted reactivity and capacity to generate diverse derivatives enhance their worth in scientific and industrial settings. Ongoing research endeavors focus on unveiling novel synthetic methodologies and expanding the applications of hydrazides, thereby reinforcing their significance within the realm of chemistry. The noteworthy bioactivity of α-benzilmonoxime and its diverse derivatives is widely acknowledged. As an example, the central nervous system is strongly stimulated by α-benzilmonoximehydrazide, and it is widely used as a stimulant for the respiratory system [14–17]. Building upon this knowledge and our sustained interest in innovating new α-benzilmonoxime compounds, complexes with the ligand benzilmonoximehydrazide-*m*-chlorobenzaldehyde (HBMH*m*CB) are described in this communication, along with their synthesis and characterization.

EXPERIMENTAL:

The analytical reagent (AR) quality chemicals and solvents were used without any further processing. An analyzer from the Thermo Finning FLASH-1112 series was used to look at the HBMH*m*CB complexes. Metal complexes' metal contents were determined via gravimetric analysis. Using $[Co(Hg(SCN)_4]$ as a standard, the magnetic susceptibility of trivalent metal complexes was evaluated at 301K using a Gory balance. A Perkin-Elmer Spectrum-100 model FT-IR spectrophotometer was used to gather FT(IR) spectra in the solid state, while a JASCO UV-visible spectrophotometer was used to capture UV-visible spectra. The results were acquired by employing Cu Kα radiation in a Rigaku D/max X-ray diffractometer.

SYNTHESIS OF HBMH*M*CB LIGAND:

A warm solution containing 10 mmol of benzilmonoximehydrazide in 100 mL of ethanol received the addition of an ethanolic solution containing 12.50 mmol of *m*-chlorobenzaldehyde and 5 ml concentrated HCl. After the reaction was complete, the mixture was refluxed for five hours. Upon cooling, a yellow precipitate formed, which was then filtered and rinsed with hot water. The raw material underwent recrystallization from methanol, yielding 28.82 grams (79.83%) of pure HBMH*m*CB.

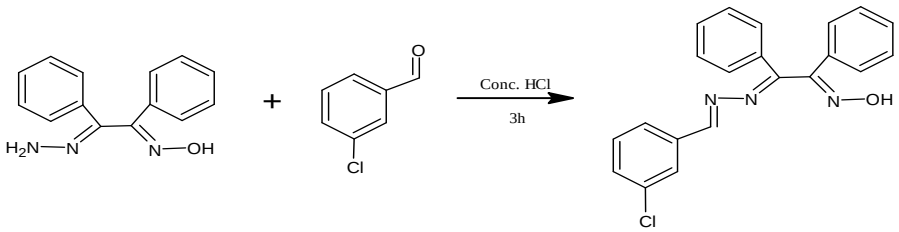

Scheme 1: Reaction scheme of HBMH*m*CB ligand

TRANSITION METAL COMPLEX SYNTHESIS:

In a pH 7 water solution, 10 mmol of HBMH*m*CB ligand ethanol and 5 mmol of metal chloride were combined. The reaction mixture was refluxed in a water bath for 10-12 hours after cooling to 28°C. The compounds with solid colors were separated by filtering them, washing them with hot distilled water, and then letting them dry on silica gel at room temperature.

$$2\text{HBMH}m\text{CB} + \text{MCl}_2.n\text{H}_2\text{O} \xrightarrow[\Delta,\ 10 - 12\text{h}]{0.1\ \text{N NaOH}} \text{M(BMH}m\text{CB)}_2 + 2\text{HCl}$$

Scheme 2: Reaction scheme of metal complexes

ANTIMICROBIAL ACTIVITY:

Several bacterial species, such as *S. aureus*, *P. aeruginosa, B. subtilis*, and *E. coli*, were tested to characterize the HBMH*m*CB ligand and its complexes. The antifungal activity of the ligand was also evaluated against *C. albicans* and *S. cerevisiae*. Using the disc diffusion method, the standard antifungal agent was fluconazole, while the common antibacterial agent was streptomycin [18]. DMSO was used to prepare the test solutions. To determine how effective the chemicals were against bacteria, the diffusion method was employed. For each organism being studied, a sterile agar medium was supplemented with half a milliliter of spore suspension (containing 106 to 107 spores ml^{-1}) just before solidification. After that, the mixture was transferred into 9-cm-diameter sterile Petri dishes and left to harden. In each plate, wells were made using a sterile corn borer that had a diameter of 6 mm. Three wells were then filled with 0.1 ml of the tested substances that had been dissolved in DMSO. For 48 hours (for bacteria) and 72 hours (for fungi), The dishes were placed in an incubator set at 37 ◦C until clear or inhibitory zones formed around every well.

RESULTS AND DISCUSSION:

The physical and analytical properties of the Schiff base ligand and its complexes are detailed in **Table 1**. Some common organic solvents are insoluble in these compounds; however, they are soluble in DMF, nitrobenzene, and DMSO. All of the complexes have a metal-to-ligand ratio of 1:2 according to the analytical results. This complex composition is represented as $[ML_2]$, where M is the chemical formula for Ni(II), Fe(II), Pd(II), Co(II), Cu(II), Mn(II), Hg(II), Cd(II), and Zn(II), and L_2 is the formula for HBMH*m*CB. The fact that their molar conductance values are very low in nitrobenzene solutions with a concentration of 10^{-3} M (as indicated in **Table 1**) indicates that they are not electrolytic [19].

Table 1: The HBMH*m*CB ligand and its metal complexes: analytical and physical data

Compound	Colour	Yield %	M.P. / Dec. point°C	Elemental Analysis						Magnetic Moments (B.M.)	Electrical Conductance 10^{-3} M(in NB) mhos
				% M Found (Calcd)	% C Found (Calcd)	% H Found (Calcd)	% N Found (Calcd)	% O Found (Calcd)	Cl% Found (Calcd)		
HBMH*m*CB	Yellow	79.83	193	-	69.62 (69.71)	4.40 (4.46)	11.55 (11.61)	4.39 (4.42)	9.71 (9.80)	-	-
[Fe(BMH*m*CB)$_2$]	Blue	77.42	206	7.19 (7.20)	64.93 (64.96)	3.84 (3.87)	10.69 (10.83)	4.10 (4.12)	9.13 (9.15)	5.60	1.59
[Co(BMH*m*CB)$_2$]	Brown	81.59	216	7.50 (7.57)	64.66 (64.70)	3.81 (3.85)	10.73 (10.78)	4.04 (4.11)	9.09 (9.11)	5.11	0.72
[Ni(BMH*m*CB)$_2$]	Green	76.52	216	7.52 (7.54)	64.61 (64.72)	3.84 (3.85)	10.73 (10.79)	3.81 (3.85)	9.09 (9.12)	3.13	2.27
[Pd(BMH*m*CB)$_2$]	Brown	82.54	225	12.60 (12.83)	60.96 (61.02)	3.55 (3.63)	10.10 (10.17)	3.86 (3.87)	8.57 (8.60)	-	4.25
[Cu(BMH*m*CB)$_2$]	Green	79.02	227	8.10 (8.11)	62.27 (62.32)	3.80 (3.83)	10.65 (10.72)	4.06 (4.08)	9.01 (9.05)	1.93	2.21
[Zn(BMH*m*CB)$_2$]	Yellow	74.89	216	8.30 (8.33)	63.99 (64.17)	3.76 (3.82)	10.64 (10.70)	4.03 (4.07)	9.02 (9.04)	-	1.56
[Mn(BMH*m*CB)$_2$]	Brown	74.12	216	9.11 (9.16)	64.99 (65.04)	3.80 (3.87)	10.79 (10.84)	4.09 (4.13)	9.11 (9.16)	5.04	0.73
[Cd(BMH*m*CB)$_2$]	Yellow	78.54	227	13.13 (13.50)	60.20 (60.55)	3.47 (3.60)	10.00 (10.09)	3.82 (3.84)	13.43 (13.50)	-	2.25
[Hg(BMH*m*CB)$_2$]	Red	73.47	236	23.77 (24.10)	60.11 (60.55)	3.54 (3.60)	10.01 (10.09)	3.81 (3.84)	8.48 (8.53)	-	2.40

INFRARED SPECTRA:

The infrared spectral information is presented in **Table 2.** The free ligand exhibits strong broadband at 3388 cm-1, which is a result of the v(N-OH) vibration. All complexes lack this characteristic, which suggests that the oxime's hydroxyl group was deprotonated when the complex was formed [20-22]. The strong peak seen at 1630 cm^{-1} in the Schiff base ligand is the stretching vibration of the v(C=N) azomethine. According to references [23–24], when the azomethine nitrogen atom coordinated with the central metal ion, this peak shifted to a lower frequency between 1571 and 1594 cm^{-1}.
These observations are additionally substantiated by the emergence of fresh bands at 519-559 cm^{-1}, and 504-517 cm^{-1} in the complexes. These bands were designated for the v(M-N), as well as the v(M-N) stretching vibrations, respectively [25-26]. There is no change in the complex spectra for the ligand's absorption band (840-846 cm^{-1}) that is associated with C-Cl, suggesting that it is not involved in coordination [27].

Table 2: The FT(IR) spectral bands of the ligand (HBMHmCB) and its metal complexes (cm^{-1}):

Assignments	HBMHmCB	Fe(II)	Co(II)	Ni(II)	Pd(II)	Cu(II)	Zn(II)	Cd(II)	Hg(II)	Mn(II)
vOH Oximino	3388	-	-	-	-	-	-	-	-	-
vC=C Ar.	3051	3054	3056	3057	3057	3057	3053	3062	3055	3053
vC=NN	1630	1593	1597	1562	1594	1594	1594	1574	1571	1578
vC=NO	1513	1493	1491	1446	1493	1490	1492	1447	1446	1493
vN-N	1008	1001	1091	1000	1028	1022	1008	1023	1021	1023
vN→O	-	985	996	969	999	1000	988	997	989	1009
vM-N	-	534	559	536	519	536	535	530	552	535
vM→N	-	507	516	508	509	519	504	517	510	512

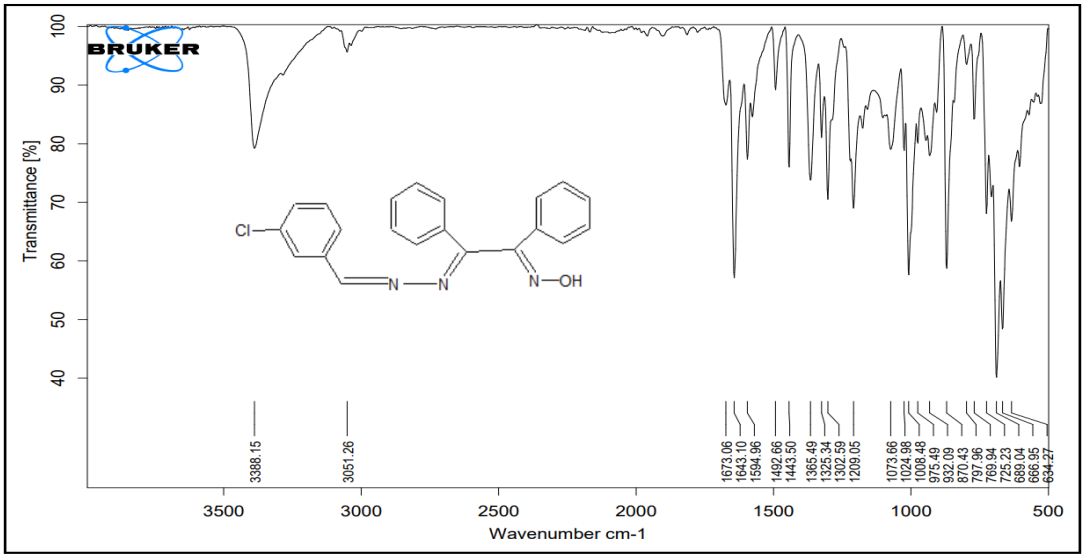

Figure 1: FT(IR) spectrum of HBMH*m*CB ligand

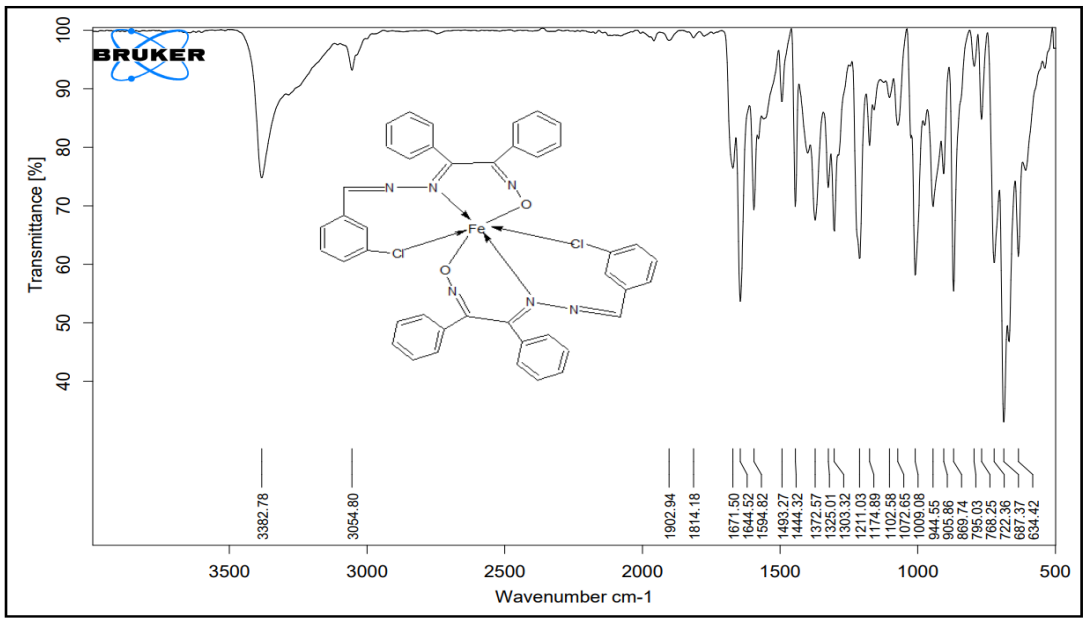

Figure 2: FT(IR) spectrum of [Fe(BMH*m*CB)$_2$] complex

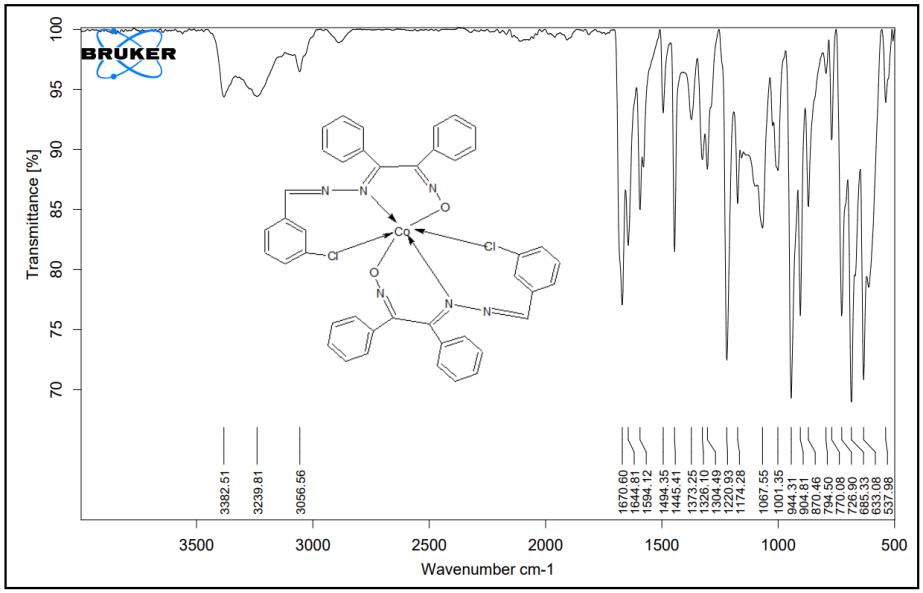

Figure 3: FT(IR) spectrum of [Co(BMH*m*CB)$_2$] complex

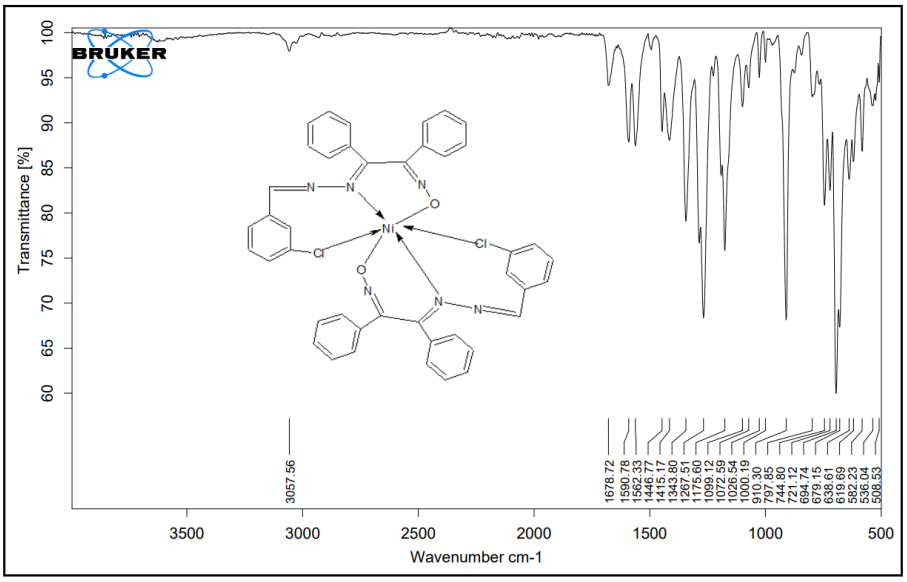

Figure 4: FT(IR) spectrum of [Ni(BMH*m*CB)$_2$] complex

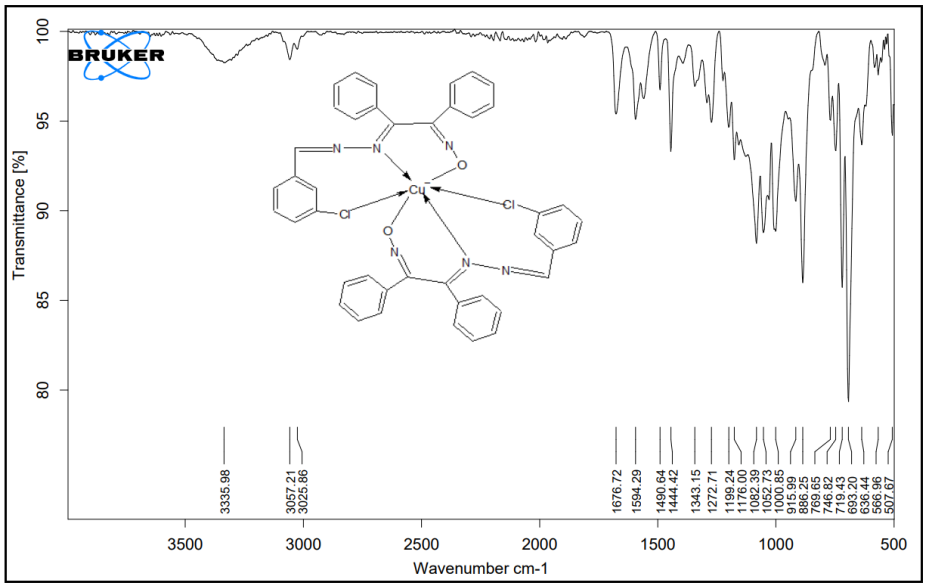

Figure 5: FT(IR) spectrum of [Cu(BMH*m*CB)$_2$] complex

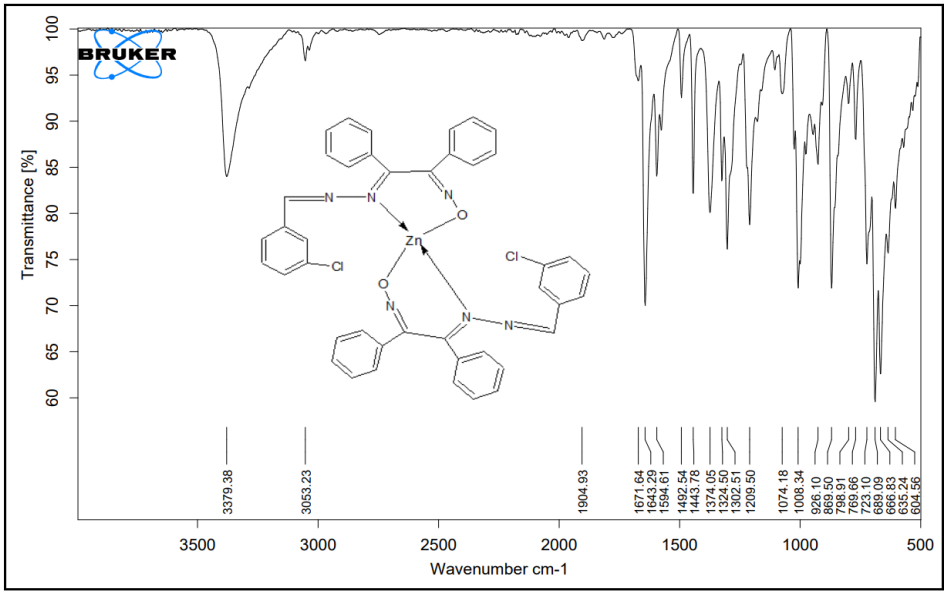

Figure 6: FT(IR) spectrum of [Zn(BMH*m*CB)$_2$] complex

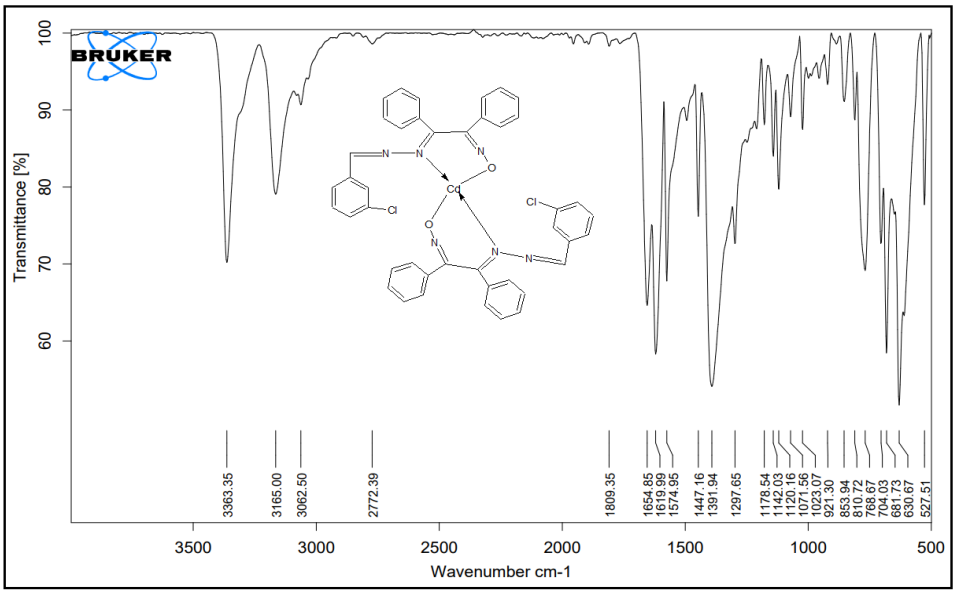

Figure 7: FT(IR) spectrum of [Cd(BMH*m*CB)$_2$] complex

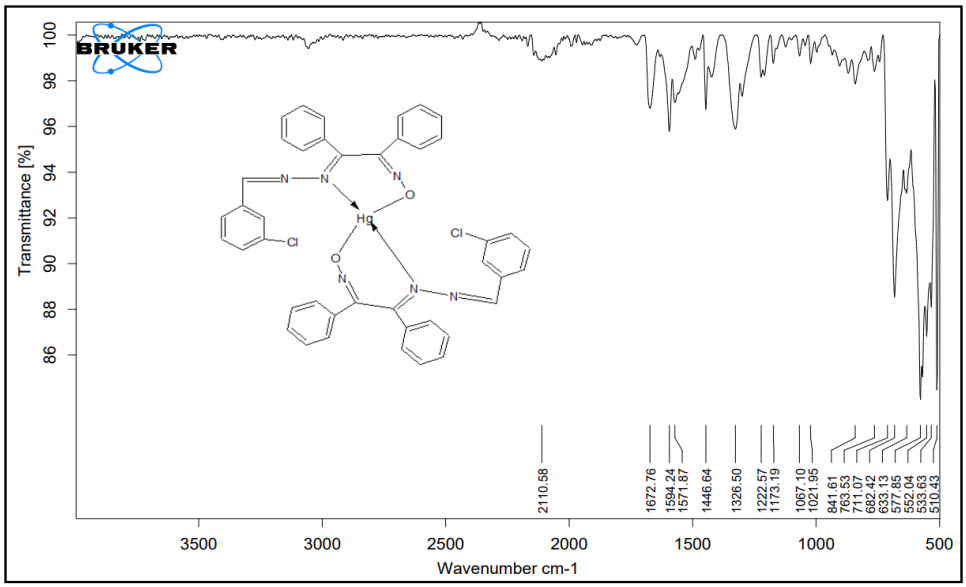

Figure 8: FT(IR) spectrum of [Hg(BMH*m*CB)$_2$] complex

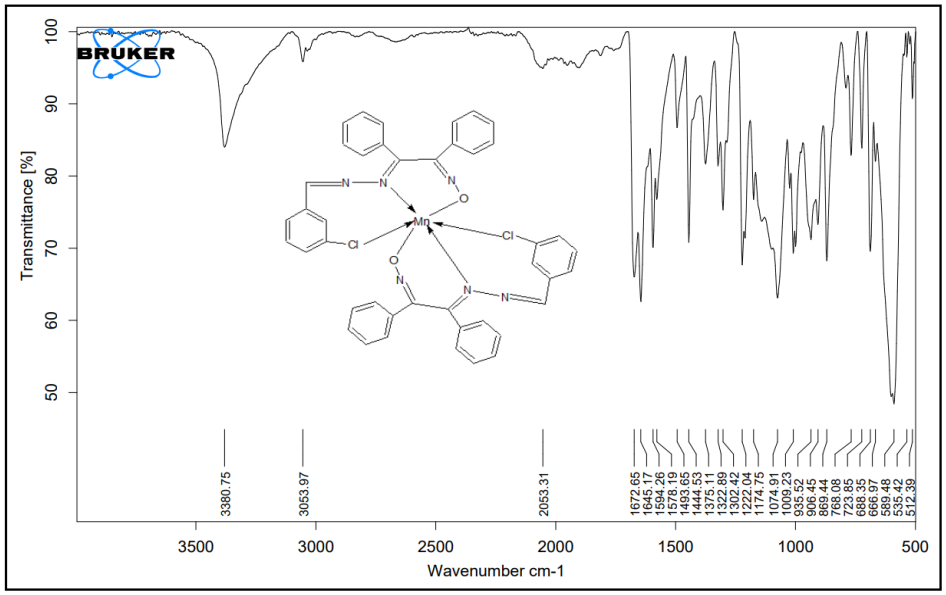

Figure 9: FT(IR) spectrum of [Mn(BMH*m*CB)$_2$] complex

^{1}H-NMR SPECTRA:

In the 1H-NMR spectra, the phenyl groups that correspond to the aromatic area at 7.424-8.623 ppm are shown by the HBMHmCB ligand and its Pd(II), Zn(II), Hg(II), and Cd(II) complexes. The singlet signal at 12.417 ppm—associated with the N-OH proton—is absent in the Pd(II), Zn(II), Hg(II), and Cd(II) complexes of the HBMHmCB ligand, suggesting that the oxime's hydroxyl group has been deprotonated in the ligand [28].

Table 3: HBMHmCB ligand and complexes PMR spectrum

Compound	N-OH	=CH-	Aromatic Proton
HBMH*m*CB	12.417	10.591	7.425-8.057
[Pd(BMH*m*CB)$_2$]	-	11.602	7.424-8.213
[Zn(BMH*m*CB)$_2$]	-	12.428	7.430-8.195
[Cd(BMH*m*CB)$_2$]	-	12.246	7.477-8.623
[Hg(BMH*m*CB)$_2$]	-	11.588	7.273-8.380

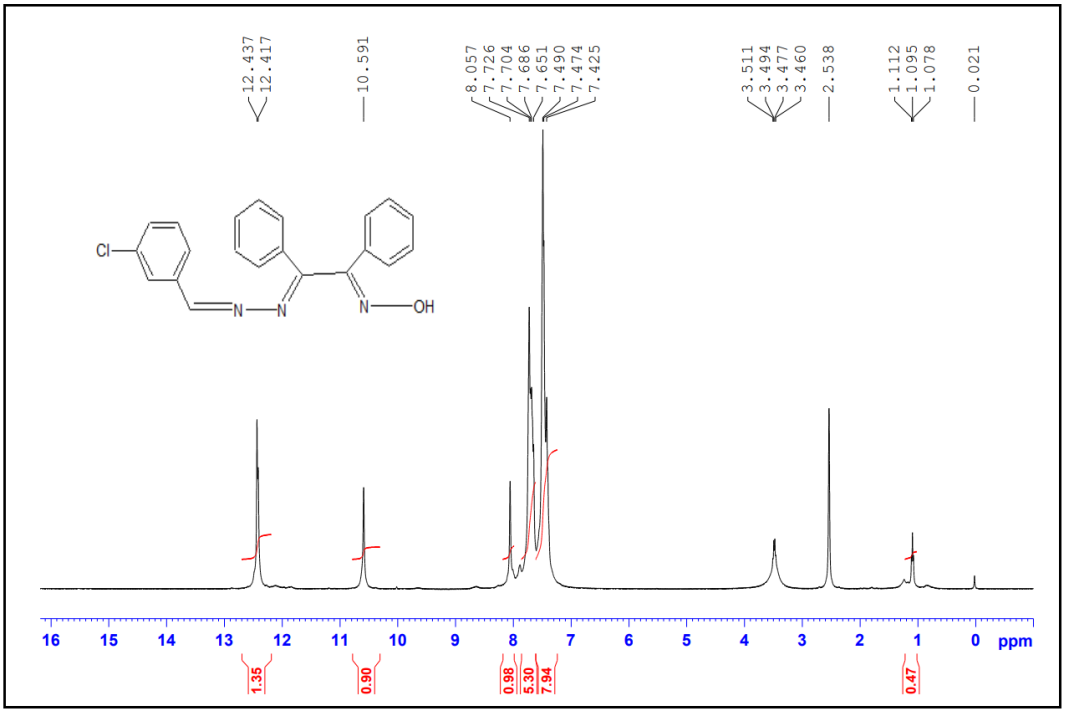

Figure 10: PMR spectrum of HBMH*m*CB ligand

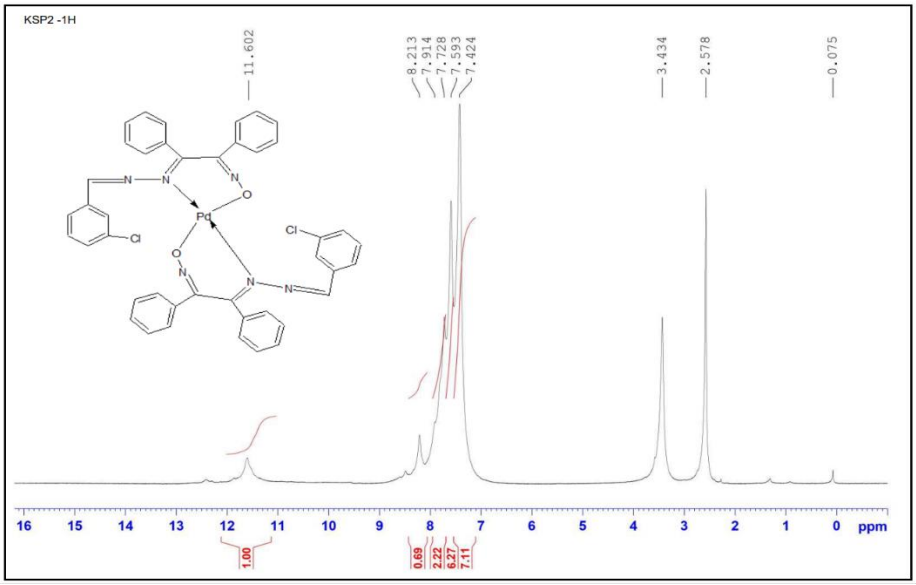

Figure 11: FT(IR) spectrum of [Pd(BMH*m*CB)$_2$] complex

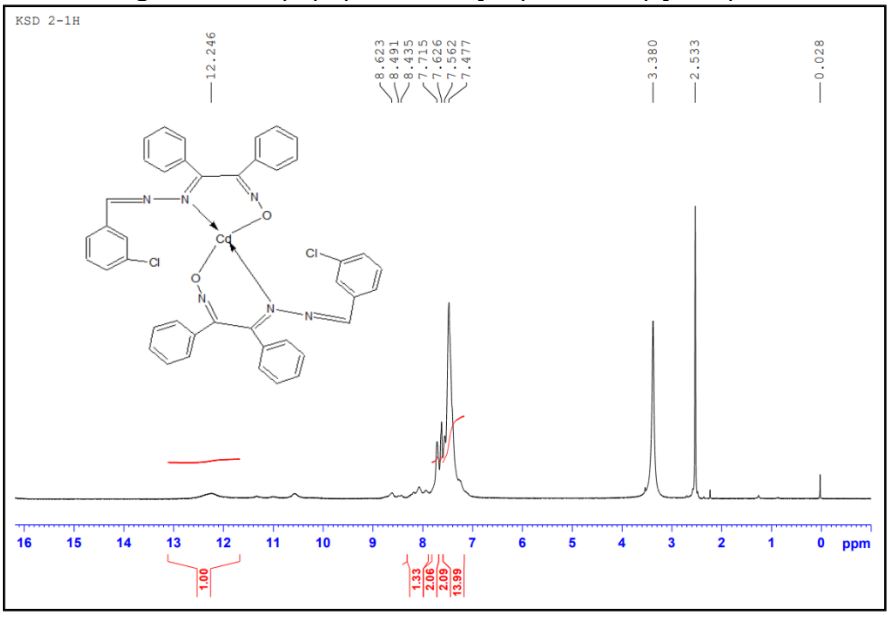

Figure 12: FT(IR) spectrum of [Cd(BMH*m*CB)$_2$] complex

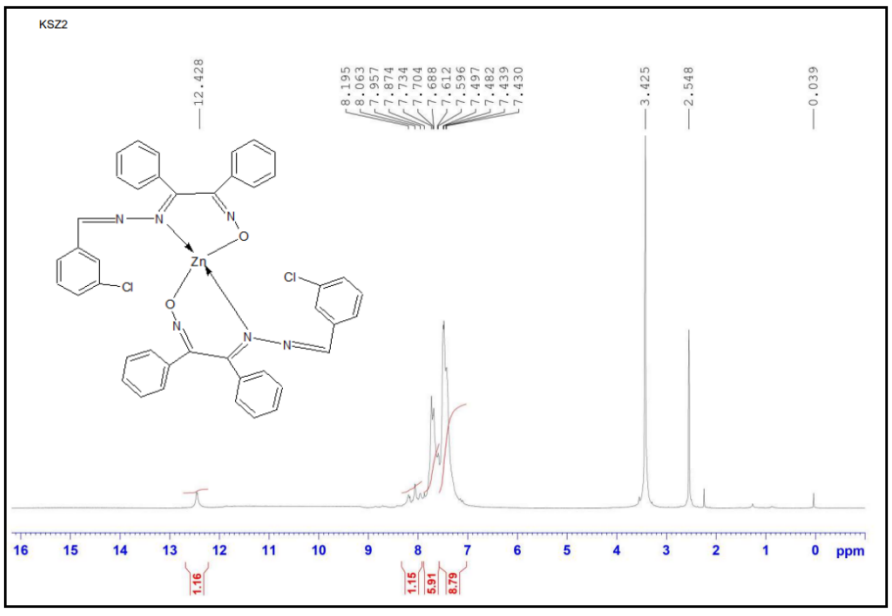

Figure 13: FT(IR) spectrum of [Zn(BMH*m*CB)$_2$] complex

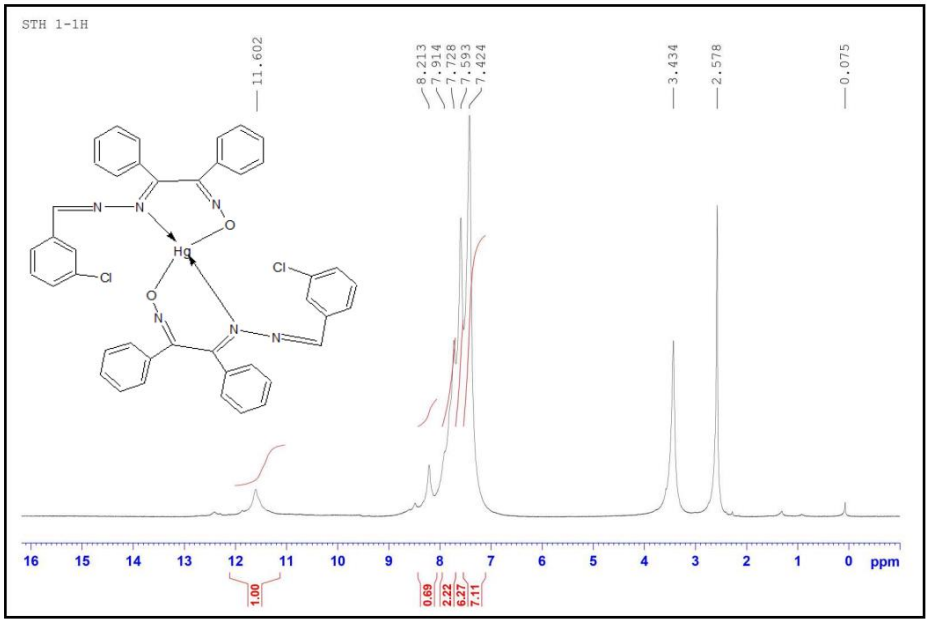

Figure 14: FT(IR) spectrum of [Hg(BMH*m*CB)$_2$] complex

ELECTRONIC SPECTRA AND MAGNETIC MOMENT:

Measurements of the PMR spectrum The complexes' magnetic moments and electronic spectrum bands are listed in Table 3. Absorption bands at 246-269 nm and 363-369 nm with high molar extinction coefficients, corresponding to π□π* and n□π* intra-ligand charge transfer, respectively, are shown in the electronic spectra of HBMHmCB and its = Fe(II), Co(II), Ni(II), Pd(II), Cu(II), Zn(II), Hg(II), Cd(II), and Mn(II) complexes in DMF. These intense absorption bands meet the Lapport selection requirements. One broadband at 546 nm appears in the Fe(II) complex's electronic spectrum; this is likely due to the 5T2g 5Eg transition. Complexes involving the ligand HBMHmCB and Pd(II) Octahedral geometry is consistent with this finding [29, 30].

In an octahedral setting, the Mn(II) complex displays bands that are spin-and parity-forbidden. Three extra bands at 578 nm, 481 nm, and 353 nm are visible in the electronic spectra of the Mn(II) complex in DMF, in addition to the * and n* transitions. According to reference [31], these are attributed to the transitions 6A1g 4T1g(G), 6A1g 4T2g(G), and 6A1g 4T1g(P)]. Regardless of temperature, the nearly spin-only magnetic moment of 5.9 B.M. in Mn(II) with a high spin d5 structure remains constant. As predicted, the Mn(II) complex has a magnetic moment of 5.04 B.M., lending credence to the idea that the metal ion is surrounded by an octahedral geometry [32].

Three medium-intensity bands at 898 nm, 608 nm, and 553 nm make up the electronic spectra of the Co(II) complex in DMF. The transitions 4T1g 4T2g(F), 4T1g 4T1g(P), and 4T1g 4A2g(F) are each given these values. Using the effective symmetry of an octahedral environment, the electronic spectra of these complexes are explained [33-34].

The first and second ligand field transitions, 3A2g 3T2g and 3A2g 3T1g, respectively, are attributed to the bands seen at 973 nm and 678 nm (18690 cm-1) in the nickel(II) complex. According to the Tanabe-Sugano diagram, O/B is equal to 21, and the second-to-first transition ratio, 2/1 = 18690 cm-1/13440 cm-1, is 1.44. This number was used to calculate the following parameters for the nickel(II) complex: Racah parameter, splitting energy, undetected third transition, and nephelauxetic parameter: 610 cm-1, 13440 cm-1, 28280 cm-1, and = 0.608 [35-36].

The electronic transition from type 2Eg 2T2g is anticipated to occur in Cu(II) with a d9 structure. The Cu(II) complex exhibited two Jahn-Teller distorted absorption bands at 633 nm and 622 nm, which were determined to correspond to the 2B1g 2B2g and 2B2g 2Eg transitions, respectively. In agreement with the magnetic moment seen in octahedral Cu(II) complexes, the Cu(II) complex has a magnetic moment of 1.93 B.M. These complexes contain an MN4O2 chromophore octahedral geometry and a C3 point group; thus, their electronic spectra are analyzed with effective symmetry in mind [37-38].

Oximinomethine and azomethine transition bands were observed in the 263-308 nm region of the electronic spectra of Pd(II), Zn(II), Cd(II), and Hg(II) complexes. The complex spectra show less intense and broad bands spanning 349-438 nm due to the overlap between low-energy π → π* transitions, which are mainly located within the azomethine group, and LMCT (ligand-to-metal charge transfer) transitions, which originate from the lone pairs of the oximino oxygen donor to Pd(II), Zn(II), Cd(II), and Hg(II).

Table 4: HBMHmCB ligand electronic absorption spectrum data and its metal complexes

Compound	λnm	ε (dm³/mol/cm)	Transition
HBMH*m*CB	343	9878	$\pi \rightarrow \pi^*$
	286	10547	$\pi \rightarrow \pi^*$
[Fe(BMH*m*CB)$_2$]	546	579	$^5T_{2g} \rightarrow {}^5E_g$
	378	8267	LMCT
	311	5499	LMCT
[Co(BMH*m*CB)$_2$]	898	8	$^4T_{1g}(F) \rightarrow {}^4T_{2g}(F)$ (ν_1)
	608	1387	$^4T_{1g} \rightarrow {}^4T_{2g}$ (ν_2)
	553	938	$^4T_{1g}(F) \rightarrow {}^4T_{2g}(P)$ (ν_3)
[Ni(BMH*m*CB)$_2$]	973	82	$^3A_{2g}(F) \rightarrow {}^3T_{2g}(F)$ (ν_1)
	678	339	$^3A_{2g}(F) \rightarrow {}^3T_{1g}(F)$ (ν_2)
	535	798	$^3A_{2g}(F) \rightarrow {}^3T_{1g}(P)$ (ν_3)
[Pd(BMH*m*CB)$_2$]	378	11021	MLCT
	302	19923	MLCT
	246	15238	MLCT
[Cu(BMH*m*CB)$_2$]	633	942	$^2B_{1g} \rightarrow {}^2A_{1g}(d_{x2-y2} \rightarrow d^2_z)$ (ν_1)
	622	103	$^2B_{1g} \rightarrow {}^2B_{2g}(d_{x2-y2} \rightarrow d_{zy})$ (ν_2)
	456	19533	$^2B_{1g} \rightarrow {}^2E_g(d_{x2-y2} \rightarrow d_{zy}, d_{yz})$ (ν_3)
[Zn(BMH*m*CB)$_2$]	423	19923	LMCT
	349	22618	LMCT
	263	26783	LMCT
[Cd(BMH*m*CB)$_2$]	376	5963	LMCT
	308	9987	LMCT
	269	10003	LMCT
[Hg(BMH*m*CB)$_2$]	438	14997	LMCT
	349	20639	LMCT
	244	24722	LMCT
[Mn(BMH*m*CB)$_2$]	578	263	$^6A_{1g} \rightarrow {}^4T_{1g}$ (^4G) (ν_1)
	481	478	$^6A_{1g} \rightarrow {}^4E_g$ (^4G) (ν_2)
	353	8266	$^4A_{1g}$ (^4G) (10B+5C) $^6A_{1g} \rightarrow {}^4E_g$ (^4D) (ν_3)

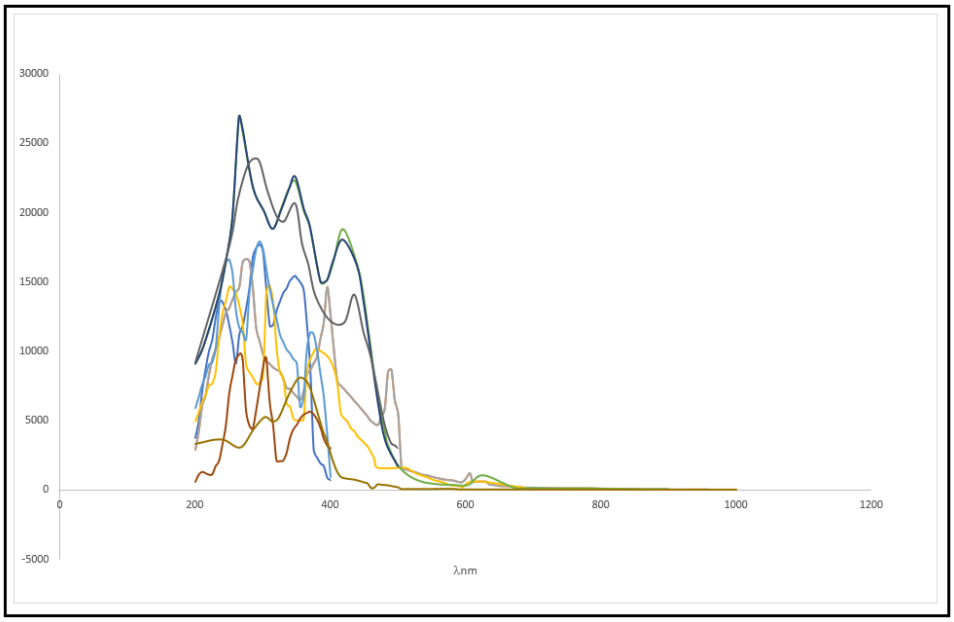

Figure 15: UV-visible spectra of HBMH*m*CB ligand and its metal complexes

ESR SPECTRUM:

The EPR spectra of the Cu(II) complex were recorded both in a polycrystalline sample and in a DMF solution. In both the parallel and perpendicular 63Cu areas, this spectrum exhibits a distinct anisotropic signal. The recorded data show values for $g_\perp$ in the range of 2.0021–2.1301 and for $g_{||}$ in the range of 2.0053–2.2299. According to [39], the copper(II) complex is much distorted from Oh symmetry to D4h symmetry since the g-values are close to 2 and $g|| > g\perp > 2.0023$.

The exchange interaction between the copper centers in a polycrystalline solid has been measured by computing a parameter G = (g□O − 2)/(g⊥ − 2). According to Hathaway [27,28], the exchange contact is considered minor if G > 4, however a large exchange interaction in the solid complexes is indicated by a G < 4. The solid complexes described in this work display exchange contact, as the 'G' values are smaller than 4.

POWDER XRD:

In the 2θ = 20-80◦ range, X-ray diffraction patterns of the complexes were recorded. The absence of peaks in the complexes suggests their amorphous characteristics [40].

ANTIMICROBIAL ACTIVITY:

Table 5 displays the ligand and complex antibacterial and antifungal characteristics. A higher concentration of the complex-containing test solution is associated with an increase in activity [41]. The antibacterial activity of the metal complexes is higher than that of the Schiff base ligands, as seen in **Table 6**. When it comes to killing gram-positive and gram-negative bacteria, the Cu(II) complex stands out among the other three complexes. Table 4 shows that the fungicidal screening findings show that the Cu(II) and Ni(II) complexes are moderately active when compared to other complexes and the Schiff base ligand.

Table 5: Antibacterial data of HBMHmCB ligand and its metal complexes

Compound	Antibacterial Activity (zone of inhibition)			
	S. aureus	***B. subtilis***	***E. coli***	***P. aeruginosa***
HBMH*m*CB	9	7	8	7
[Fe(BMH*m*CB)$_2$]	11	14	15	0
[Co(BMH*m*CB)$_2$]	16	15	17	12
[Ni(BMH*m*CB)$_2$]	19	16	18	15
[Pd(BMH*m*CB)$_2$]	21	15	15	12
[Cu(BMH*m*CB)$_2$]	26	24	20	19
[Zn(BMH*m*CB)$_2$]	13	18	0	6
[Mn(BMH*m*CB)$_2$]	12	13	0	19
[Cd(BMH*m*CB)$_2$]	12	13	16	17
[Hg(BMH*m*CB)$_2$]	15	16	12	9
Streptomycin	10	7	13	8

Table 6: Antifungal data of HBMHmCB ligand and its metal complexes

Compound	Antifungal Activity (zone of inhibition)	
	C Albican	***S. C.***
HBMH*m*CB	7	6
[Fe(BMH*m*CB)$_2$]	15	13
[Co(BMH*m*CB)$_2$]	16	17
[Ni(BMH*m*CB)$_2$]	19	20
[Pd(BMH*m*CB)$_2$]	9	11
[Cu(BMH*m*CB)$_2$]	11	9
[Zn(BMH*m*CB)$_2$]	12	10
[Mn(BMH*m*CB)$_2$]	17	11
[Cd(BMH*m*CB)$_2$]	22	9
[Hg(BMH*m*CB)$_2$]	13	18
Fluconazole	10	8

CONCLUSION:

The Schiff base ligand HBMHmCB is denoted by the symbol [ML2] in compounds formed by transition metal complexes. L is proven to be a tridentate ligand according to the data. The complexes of Fe(II), Mn(II), Co(II), Cu(II), and Ni(II) exhibit octahedral geometry, those of Cd(II), Hg(II), and Zn(II) exhibit tetrahedral geometry, and the complex of Pd(II) takes on a square planar shape. According to the results of the antibacterial activities, the Cu(II) complex is the most effective of the metal complexes tested.

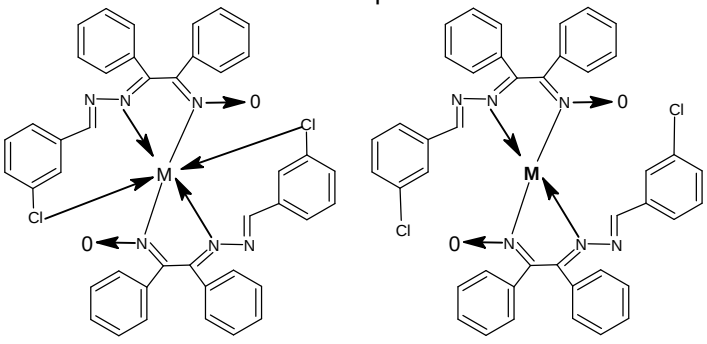

a **b**

Where M = (a) Fe(II), Co(II), Ni(II), Cu(II), Mn(II) and (b) Pd(II), Zn(II), Cd(II), Hg(II)

Figure 2: Tentatively structures of the metal complexes

References:

1. P. Reddy, K. Reddy, *Polyhedron*. **2000,** *19*(14), 1687-1692. https://doi.org/10.1016/S0277-5387(00)00429-0
2. V. Sharma, S. Srivastava, *Synthesis and Reactivity in Inorganic, Metal-Organic and Nano-Metal Chemistry*. **2005,** *35*(4), 311-318. https://doi.org/10.1081/SIM-200055249
3. A. Ensafi, H. Eskandari. *Microchemical Journal*, **1999,** *63*(2), 266-275. https://doi.org/10.1006/mchj.1999.1790
4. R. Badekar, S. Kulkarni, R. Lokhande, B. Thawkar, *International Journal of Applied Research*. **2016,** *2*(9), 175-179.
5. E. Soleimani, *Journal of the Chinese Chemical Society*. **2011,** *58*(1), 53-59. https://doi.org/10.1002/jccs.201190058
6. H. Eskandari, G. Karkaragh, *Bulletin-Korean Chemical Society*. **2003,** *24*(12), 1731-1736.
7. S. Vedanayaki, P. Jayaseelan, *European Journal of Chemistry*. **2016,** *7*(3), 368-374. https://doi.org/10.5155/eurjchem.7.3.368-374.1443
8. V. Sharma, S. Srivastava, *Synthesis and Reactivity in Inorganic, Metal-Organic and Nano-Metal Chemistry*. **2005,** *35*(4), 311-318. https://doi.org/10.1081/SIM-200055249
9. S. Sankhe, Reaction of p-chlorobenzaldehyde derived ligand Complexes possessing an azomethine and oximino functions with Lanthanide (III) ions and its biological activity. **2023.** https://doi.org/10.21203/rs.3.rs-2565335/v1
10. M. Lauwiner, P. Rys, J. Wissmann, *Applied Catalysis A: General*. **1998,** *172*(1), 141-148. https://doi.org/10.1016/S0926-860X(98)00110-0
11. S. Rohane, A. Makwana, *Asian Journal of Research in Chemistry*. **2017,** *10*(4), 417-430. https://doi.org/10.5958/0974-4150.2017.00070.0
12. G. Byrkit, G. Michalek, *Industrial & Engineering Chemistry*. **1950,** *42*(9), 1862-1875. https://doi.org/10.1021/ie50489a046
13. J. Troyan, *Industrial & Engineering Chemistry*. **1953,** *45*(12), 2608-2612. https://doi.org/10.1021/ie50528a020
14. R. Bhagwat, R. Badekar, K. Jain, R. Lokhande, *Journal of Advanced Scientific Research*. **2021,** *12*(02 Suppl 1), 230-234.
15. R. Bhagwat, R. Badekar, K. Jain, R. Lokhande, *Journal of Advanced Scientific Research*, **2021,** *12*(02 Suppl 1), 225-229.
16. S. Chaugule, R. Badekar, R. Lokhande, *JETIR*, **2019,** *6(5)*, 1073-1075.
17. P. Yadav, R. Badekar, P. Nag, R. Lokhande, *Journal of Advanced Scientific Research*, **2021,** *12*(01), 231-234. https://doi.org/10.55218/JASR.202112130.
18. P. Pandey, A. Mehta, S. Hajra, *Journal of phytology*. **2011,** *3*(3), 92-95.
19. I. Ali, W. Wani, K. Saleem, *Synthesis and reactivity in inorganic, metal-organic, and nano-metal chemistry*. **2013,** *43*(9), 1162-1170. https://doi.org/10.1080/15533174.2012.756898
20. V. Fain, B. Zaitsev, M. Ryabov, P. Strashnov, *Russian Journal of General Chemistry*. **2010,** *80*, 1986-1995. https://doi.org/10.1134/S107036321010018X
21. Z. Zhang, G. Helms, S. Clark, G. Tian, P. Zanonato, L. Rao, *Inorganic chemistry*. **2009,** *48*(8), 3814-3824. https://doi.org/10.1021/ic8018925
22. E. Alvarez, J. Brodbelt, *Journal of the American Society for Mass Spectrometry*. **1998,** *9*(5), 463-472. https://doi.org/10.1016/S1044-0305(98)00007-5
23. M. Odabaşoğlu, Ç. Albayrak, R. Özkanca, F. Aykan, P. Lonecke, *Journal of Molecular Structure*. **2007,** *840*(1-3), 71-89. https://doi.org/10.1016/j.molstruc.2006.11.025
24. A. Sarwar, S. Saharin, H. Bahron, Y. Alias, *Journal of Luminescence*. **2020,** *223*, 117227. https://doi.org/10.1016/j.jlumin.2020.117227.
25. C. Barraclough, J. Lewis, R. Nyholm, *Journal of the Chemical Society (Resumed)*. **1959,** 3552-3555.
26. T. Yamabe, K. Hori, T. Minato, K. Fukui, *Inorganic Chemistry*. **1980,** *19*(7), 2154-2159. https://doi.org/10.1021/ic50209a063.
27. L. Andrews, *The Journal of Chemical Physics*. **1968,** *48*(3), 979-982. https://doi.org/10.1063/1.1668853
28. I. Fritsky, R. Lampeka, V. Skopenko, Y. Simonov, A. Dvorkin, T. Malinowsky, *Zeitschrift für Naturforschung B*. **1993,** *48*(3), 270-276. https://doi.org/10.1515/znb-1993-0304
29. S. Xu, J. Smith, S. Gozem, A. Krylov, J. Weber, *Inorganic Chemistry*. **2017,** *56*(12), 7029-7037. https://doi.org/10.1021/acs.inorgchem.7b00620
30. L. Latos-Grazynski, J. Lisowski, M. Olmstead, A. Balch, *Inorganic Chemistry*. **1989,** *28*(6), 1183-1188. https://doi.org/10.1021/ic00305a032
31. L. Chai, L. Tang, L. Chen, J. & Huang, *Polyhedron*. **2017,** *122*, 228-240. https://doi.org/10.1016/j.poly.2016.11.032
32. R. Ammar, A. Alaghaz, M. Zayed, l. Al-Bedair, *Journal of Molecular Structure*. **2017,** *1141*, 368-381. https://doi.org/10.1016/j.molstruc.2017.03.080
33. S. Chandra, L. Gupta, D. Jain, *Spectrochimica Acta Part A: Molecular and Biomolecular Spectroscopy*. **2004,** *60*(10), 2411-2417. https://doi.org/10.1016/j.molstruc.2017.03.080
34. M. Al-Omair, *Arabian Journal of Chemistry*. **2019,** *12*(7), 1061-1069. https://doi.org/10.1016/j.molstruc.2017.03.080
35. Yu, X., Wang, N., He, H., & Wang, L. (2014). Theoretical investigations of the structures and electronic spectra of Zn (II) and Ni (II) complexes with cyclohexylamine-N-dithiocarbamate. *Spectrochimica Acta Part A: Molecular and Biomolecular Spectroscopy*, *122*, 283-287.
36. N. Abdel-Ghani, M. El-Ghar, A. Mansour, *Spectrochimica Acta Part A: Molecular and Biomolecular Spectroscopy*. **2013,** *104*, 134-142. https://doi.org/10.1016/j.saa.2012.11.038
37. S. Chandra, L. Gupta, *Spectrochimica Acta Part A: Molecular and Biomolecular Spectroscopy*. **2005,** *61*(1-2), 269-275. https://doi.org/10.1016/j.saa.2012.11.038
38. L. Abdel-Rahman, A. Abu-Dief, H. Moustafa, S. Hamdan, *Applied Organometallic Chemistry*. **2017,** *31*(2), e3555. https://doi.org/10.1002/aoc.3555
39. N. Hall, M. Orio, M. Gennari, C. Wills, F. Molton, C., Philouze, C. Duboc, *Inorganic Chemistry*. **2016,** *55*(4), 1497-1504. https://doi.org/10.1021/acs.inorgchem.5b02287
40. K. Buldurun, N. Turan, E. Bursal, A. Aras, A. Mantarcı, N. Çolak, I. Gülçin, *Journal of Biomolecular Structure and Dynamics*. **2021,** *39*(17), 6480-6487. https://doi.org/10.1080/07391102.2020.1802340
41. K. Buldurun, N. Turan, A. Savcı, N. Colak, *Journal of Saudi Chemical Society*. **2019,** *23*(2), 205-214. https://doi.org/10.1016/j.jscs.2018.06.002.

Graphical Abstract

42. **Synthesis, spectroscopic and biological activities of complexes of 2-[(3-Chlorobenzylidene)hydrazinylidene]-1,2-diphenylethanimine**

43. **Sharad Sankhe[1] and Krupali Shah[1]**

44. Department of Chemistry, Patkar-Varde College, Goregaon West, Mumbai-62, India.

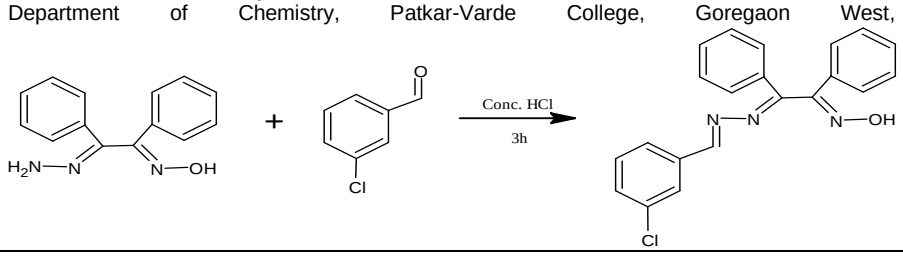

DOI: https://doi.org/10.15379/ijmst.v10i5.3633